Journal of Civil Structural Health Monitoring
https://doi.org/10.1007/s13349-021-00486-9

ORIGINAL PAPER

All-season monitoring of concrete repair in an urban tunnel in Brussels using embedded ultrasonic transducers with emphasis on robustness to environmental variations

Cédric Dumoulin[1] · **Arnaud Deraemaeker**[1]

Received: 5 January 2021 / Revised: 31 March 2021 / Accepted: 23 April 2021

Abstract
This paper presents the results of a long-term concrete monitoring campaign in an underground tunnel in Brussels. The system consists of several pairs of embedded ultrasonic piezoelectric transducers arranged in a pitch-catch configuration which have been placed in the concrete ceiling of the tunnel in areas where old concrete was demolished and then repaired. The monitoring system is fully automated and sends the recorded signals to a cloud-based system in our university where they are post-processed to extract indicators of structural changes in the monitored regions, and send automated email reports. A first period of six months is studied, during which the monitored areas have been repaired with skim mortar. The post-processing of the measured signals allows to identify clearly the time of repair in each zone and the evolution of the hardening process of the repair mortar. A second monitoring period of one year is then studied where it is found that despite the proposed improvement to the time stretching technique used to filter out the effects of changing environmental conditions, our indicators are still showing variations in periods when the temperature is very high in the tunnel. A method based on observed statistical correlations between the indicators computed in the different regions is then proposed and shown to be very efficient to remove the remaining variability and make the system very robust to environmental changes. Extreme value statistics is also presented as a tool to establish relevant thresholds for alarm-triggering with a very low level of potential false alarms. With all these developments, the monitoring system can automatically detect structural changes in the tunnel in real time while being robust to unavoidable changes in the environmental conditions in the tunnel.

Keywords Structural health monitoring · Damage detection · Embedded sensors · Ultrasonic testing · Piezoelectric sensors · Environmental effects · Extreme value statistics

Mathematics Subject Classification MSC 62

1 Introduction

Throughout the world, a large part of the civil infrastructure made of concrete was built in the 1960s and 70s and has reached the end of its theoretical lifetime of 50 years. Many of these structures made of concrete present today important pathologies and need heavy repair, often causing major disruption of traffic. Inspection and maintenance of concrete infrastructure is, therefore, currently a major concern for all infrastructure management services all around the world. The center of the city of Brussels is surrounded by a belt of underground tunnels which have been under heavy repair and renovation work for the last 5 years, after a block of concrete fell on the windshield of a car, fortunately not causing any injuries to the driver and passengers. The

This work was supported by the Brussels Region fund for R&D INNOVIRIS under the Launch Spin-off Grant No RBC/2017-SOIB-4, the Regional Public Service Brussels Mobility and by the Fonds de la Recherche Scientifique—FNRS under Grant No CDR FNRS—J0046.19.

✉ Arnaud Deraemaeker
Arnaud.Deraemaeker@ulb.be

[1] Université libre de Bruxelles (ULB), Building Architecture and Town Planning (BATir), 1050 Brussels, Belgium

Published online: 15 May 2021

repair works have been responsible for the closing of several tunnels repeatedly over the years, causing important traffic congestion, and strongly impairing mobility in the city [1].

The current strategy for inspection and repair is based on a two phase procedure. In the first phase, visual inspection is performed to identify the zones of potential damage to the concrete. This requires to remove all panels and equipment covering the concrete, and is very long and labor intensive. In the second phase, and based on the results of the first inspection, concrete core samples are extracted at different locations in the tunnel and subjected to different mechanical and chemical tests in the laboratory to determine properties such as concrete strength or depth of the carbonation front. The results of the second phase serve as a basis to decide on the repair actions that will be taken to restore the structural integrity of the tunnel.

The Rogier tunnel is a 800 m underground tunnel that is part of the belt of tunnels surrounding the city center (Fig. 1). After the two phases of inspection, a detailed plan of repair work has been set up. In the summer of 2019, in the zones of the reinforced concrete ceiling where the concrete was heavily damaged, the concrete has been removed using hydrodemolition (Fig. 2). A skim mortar (MAPEI Mageprout T60, density 2200 kg $\cdot$ m^{-3}, 28-day compressive strength $\geq$ 40 MPa) has then been applied to fill in these zones. An important issue with this kind of repair work is the necessity to obtain an excellent adhesion between the old concrete and the new one. There have been cases in the past of bad adhesion and detachment of the new concrete which required to redo the repair work. The good adhesion of concrete can be tested using a pull-out test in different testing

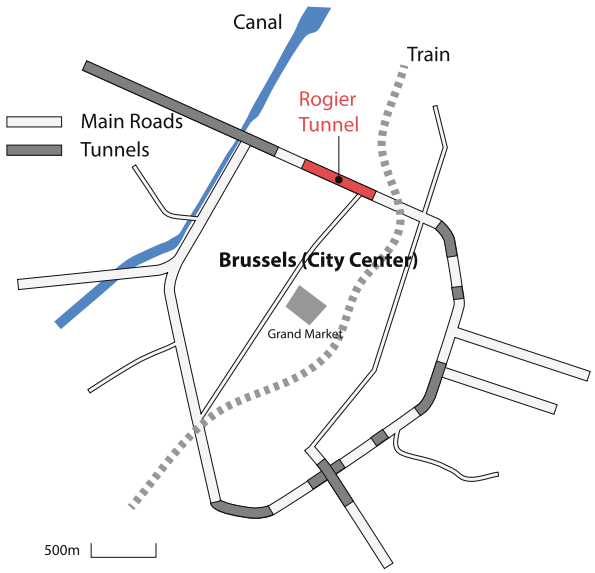

Fig. 1 The Rogier tunnel is a 800 m underground tunnel that is part of the belt of tunnels surrounding the city center

Fig. 2 General view of the zone to repair studied in the present paper. The concrete in bad state has been removed by hydro demolition

areas, after the skim mortar has hardened sufficiently. This requires manual labor and is only done at a specific time, and is partly destructive.

In the department of civil engineering (BATir) of the Université libre de Bruxelles (ULB), we have been developing a concrete monitoring technique based on pairs of embedded piezoelectric ultrasonic transducers. The transducers are a unique and optimized version of the transducers used in previous studies [2, 3] which are currently being patented. They have been originally designed to have their resonance frequency around 150 kHz with a Q-factor estimated from the electric impedance in concrete around 8. These kinds of transducers have been first proposed by a research group in the University of Houston, Texas [4]. The size of such transducers is of the same order of magnitude as the largest aggregates in concrete (Fig. 3). They have proven to provide an excellent signal-to-noise ratio thanks to the perfect coupling with the concrete (not requiring the use of a coupling gel). Other advantages of the transducers compared to

Fig. 3 Picture of the new generation of embedded piezoelectric transducers

external ones traditionally used for ultrasonic testing are the very flexible possible arrangements of the transducers pairs which are not limited to the often difficult-to-access surfaces, the repeatability of the tests due to the fixed position of the transducers once embedded in the concrete, and the possibility to do on-line remote and automated monitoring, even after panels and equipments have been placed in front of the concrete elements. They are also cost-effective compared to commercial external ultrasonic transducers (about ten times cheaper). These transducers have proven their excellent performances for monitoring concrete mechanical properties at very early age [5] and to detect cracking in three-point-bending, pull-out and cylinder compression tests [6, 7]. They have also been used to track the healing process in self-healing concrete [8]. All of these tests have been performed in the laboratory and under controlled conditions.

The goal of the *TweetCon* project financed by Innoviris in the Brussels Region was to study the field application of a monitoring system developed based on embedded piezoelectric transducers. One of the applications developed was the monitoring of concrete repair in the ceiling of the Rogier tunnel in Brussels, which is presented in this paper. Four pairs of piezoelectric transducers were embedded, each in one repaired area, and a fifth pair was embedded at a location where no repair was necessary. The transducers pairs were used in a pitch-catch mode with different types of excitation signals applied at the emitter side. Passive acoustic emission (AE) system are widely used for concrete monitoring since it allows to extract qualitative and quantitative (i.e., localization, type of cracks) evaluation of the damage [9]. This is possible at the cost of using a large network of transducers, notably to differentiate genuine and non-genuine acoustic events [10]. In contrast, using an active ultrasonic method allows to reduce the number of transducers in each monitored zone and does not require to monitor continuously to track the evolution of a damage. It will detect a change in the recorded signals even if the system was shut down at the moment of the appearance of an event. From that perspective, using an active ultrasonic system appears to be more robust against system failures and is, therefore, thought to be more appropriate for long-term monitoring systems.

The system is fully automated and sends monitoring data continuously to a cloud established in our university through a 4G mobile connection. As detailed in Sect. 2, damage indicators are then computed on the remote server based on the transmitted recorded ultrasonic signals, and a report is sent every morning by email to follow the evolution of the quality of concrete in the repaired zones.

The major difference between field applications and laboratory experiments is the exposure of the concrete to changing daily and seasonal environmental conditions. These are responsible for changes in the ultrasonic signals measured which can be of the same order of magnitude as the changes to be detected due to damage, or in this case, to skim mortar detachment from the old concrete. Such a variability in the signals can be responsible for false-positive alarms, which should be avoided at all costs. A first approach to compensate for the effects of the environment was proposed in [7]. It is based on time-stretching and was successfully applied to filter out the acoustoelastic effects in laboratory tests. The acoustoelastic effect causes a global change of wave velocity under applied stress. Although this effect is different from the ones caused by environment, it was believed that as both of them are global in nature, the same technique could be used to compensate for environmental effects. As will be detailed in Sect. 3, in the Rogier tunnel, the application of the time stretching technique to the signals was not sufficient to compensate for the changing environmental conditions. The goal of the present paper is, therefore, to present a novel and more robust approach to filter environmental effects for real-time monitoring of concrete using embedded piezoelectric transducers. It is, to the knowledge of the authors, a unique example of successful application of such techniques on field applications

The novel proposed technique is presented in Sect. 3.2. The main idea is to use a sliding average reference to perform the time stretching, rather than using always the same initial reference signal. Although this new approach strongly improves the robustness of the damage indicators to changing environmental conditions, it was not found sufficient when the tunnel is exposed to extreme temperatures as the ones we have known in the last summer of 2020, where the temperature in the tunnel was above 30°C. Therefore, in Sect. 5 we study the possibility of using an additional filtering technique which is based on the observed correlations between the different sensor pairs over a one-year period. This additional layer of filtering makes the monitoring system very robust to changing environmental conditions, even in the case of extreme temperatures.

2 Monitoring system in the Rogier tunnel

The objective of the monitoring system installed in the Rogier tunnel is to assess the quality of the repairs in the ceiling of the tunnel right after the application of the skim mortar, as well as to evaluate its long-term evolution. The embedded transducers used for that purpose are arranged by pairs in a pitch-catch configuration (Fig. 4) so that the wave is propagating from the emitter to the receiver. The wave is scattered when it encounters an heterogeneity and the signal which is measured by the receiver is therefore a signature of the actual microstructure and properties of the concrete located around the pair of transducers. If a cavity is appearing at the interface between the old and the new concrete, the wave path will be modified. This will also change

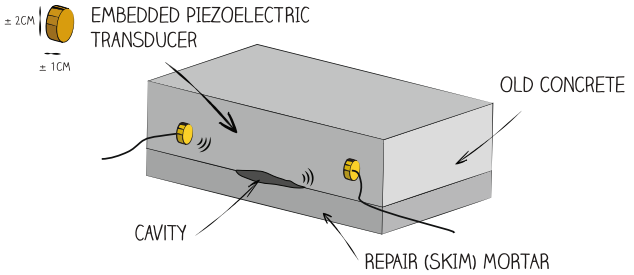

Fig. 4 Pitch-catch configuration to follow the quality of the repair with skim mortar and the potential appearance of cavities at the interface between the old and the new concrete

Table 1 Description of the pairs of transducers in the different zones, including the date at which the zone has been repaired

Zone	Emitter	Receiver	Distance (cm)	Repaired
0	SA0	SA1	43	Not repaired (Ref.)
39	SA6	SA7	69	Jun. 27 2019
40	SA4	SA5	57	Jun. 27 2019
41	SA8	SA9	63	Jul. 24 2019
38	SA10	SA11	51	Jul. 24 2019

the signal measured by the receiver, indicating a structural change. This aspect is discussed in more details in Sect. 3. Because of the difference of quality between the old concrete and the new mortar, it is expected that most of the energy of the received signal is corresponding to the part of the wave propagating in the new mortar, after the repairing mortar has hardened.

Five pairs of transducers have been installed in four repaired zones and in a control zone (without repair). The different zones are described in Table 1 where the date at which the new skim mortar has been applied is also indicated. For practical reasons, the transducers have been installed before the repair, in the old concrete, above the rebars. The fact that the wave velocity increased significantly during the curing period of the new skim mortar (see in Sect. 4) confirms the hypothesis that the early part of the wave arriving at the receiver has traveled in the new mortar, which gives an indication of its curing state. The method to set up the transducers in the old concrete is detailed in Fig. 5. The transducers are connected using coaxial cables to the data acquisition box located in a technical room of the tunnel, located in the immediate vicinity of the monitored zone.

The excitation signal is generated from a DAC board (1) and is amplified by a High Voltage Amplifier (2). The signal is then routed to a given emitter (4) through a multiplexer (switch) board (3). The emitter is then generating an ultrasonic wave which is propagating in concrete. It is caught by a receiver (5) and amplified a first time by a fixed gain AE pre-amplifier (6). The signal is then routed to the variable gain pre-amplifier (9) through a second switch board (7). The decoupling circuit (8) is used as power supply (28 VDC) of the pre-amplifiers (6) through the same line as the received signal (phantom power). The signal is then recorded by an ADC board. The actual instruments and their main characteristics (sampling frequencies, gains) are summarized in Fig. 6.

In addition to the ultrasonic system (A) described above, the temperature in measured using an RTD (resistance temperature detector) PT100 (B).

The different modules are driven by a local computer using a LabVIEW based In-House software (C). The raw data are transmitted to a cloud-based server (E) using a 4G mobile router (D) and processed by a computer located in our laboratory at ULB (F). The data transmission scheme is summarized in Fig. 7 while actual pictures of the system can be found on Figs. 5 and 8. In addition, the whole system is powered through an uninterruptible power supply (UPS) which is aimed at preventing a system outage in case of short discontinuation of the electrical grid of the tunnel. Such events were expected to happen quite often without warning during the renovation phase. The system was however not designed to support long power interruption which consequently led the system to stop the measurements when such long power interruptions occurred. This resulted in several large gaps between two successive data points in the results (e.g., see Fig. 13).

3 Signal processing and feature extraction

The different pairs of ultrasonic embedded transducers are interrogated alternatively thanks to the multiplexers (Fig. 6). The actuator of each pair is excited by different signals (i) a short pulse (10 μs) which is aimed at exciting a large frequency band and which is the one classically used in previous studies (see [7]), (ii) a Gaussian sine at 40 kHz (−6dB cutoff at 40 ± 10 Hz, i.e., approx. 4 cycles) to focus on larger wavelengths to ensure a good transmission over large distances and give a general overview of the state of the material between the emitter and the receiver, (iii) a Gaussian sine at 80 kHz (−6dB cutoff at 80 ± 20 Hz, i.e., approx. 4 cycles) to improve the sensitivity to local structural changes.

All signals have an amplitude of 80V, which appeared to be the best compromise between the performance of the power amplifier to drive accurately the capacitive loads (piezoelectric transducers and the cables) and a good signal-to-noise ratio (SNR). The SNR is also improved by adapting automatically the gain of the pre-amplifier (label 9 in Fig. 6) and by performing an average over 200 signals for each measurement.

Fig. 5 Process to install the transducers in the old concrete part of the ceiling

(a) A hole (ϕ 25 mm, 40 mm depth) is drilled in the ceiling (in the old concrete) between two reinforcement bars.

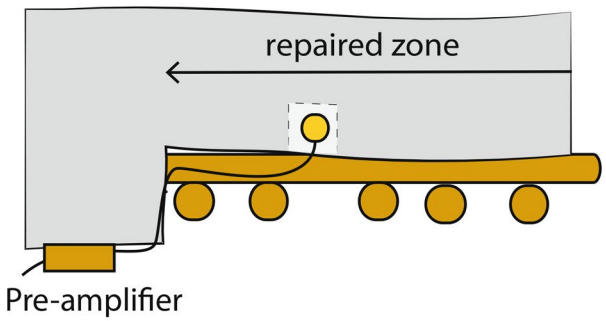

(b) The hole is partially filled with a double component epoxy grouting mortar. The transducer is pushed into it and the hole is finally filled with the epoxy grouting mortar.

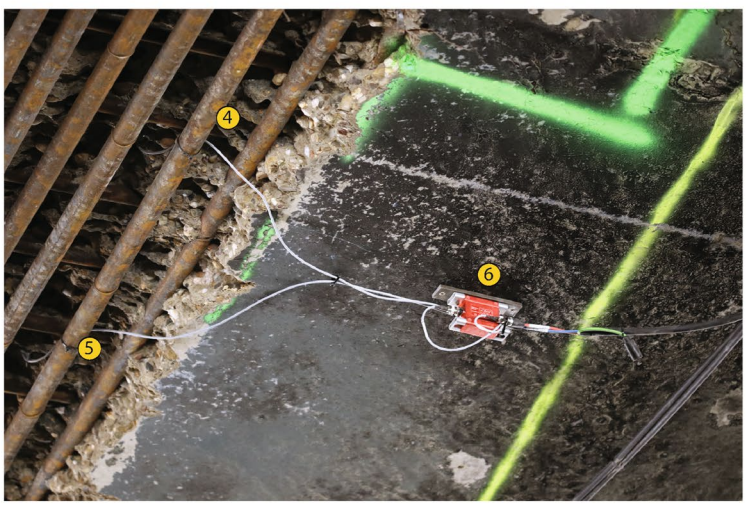

(c) The receiver is connected to a pre-amplifier.

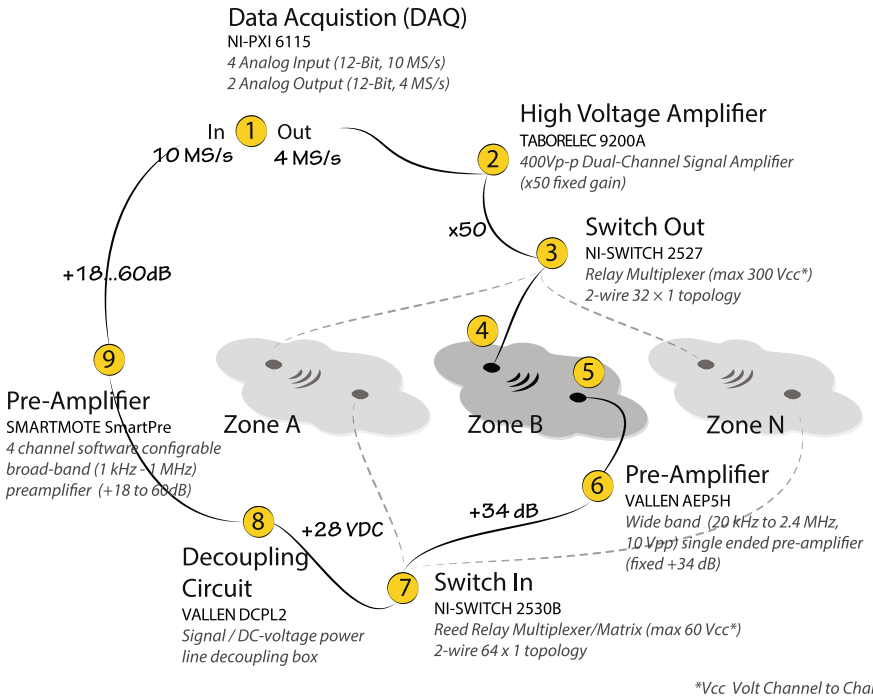

Fig. 6 Description of the instruments and connections of the Ultrasonic Data Acquisition Chain

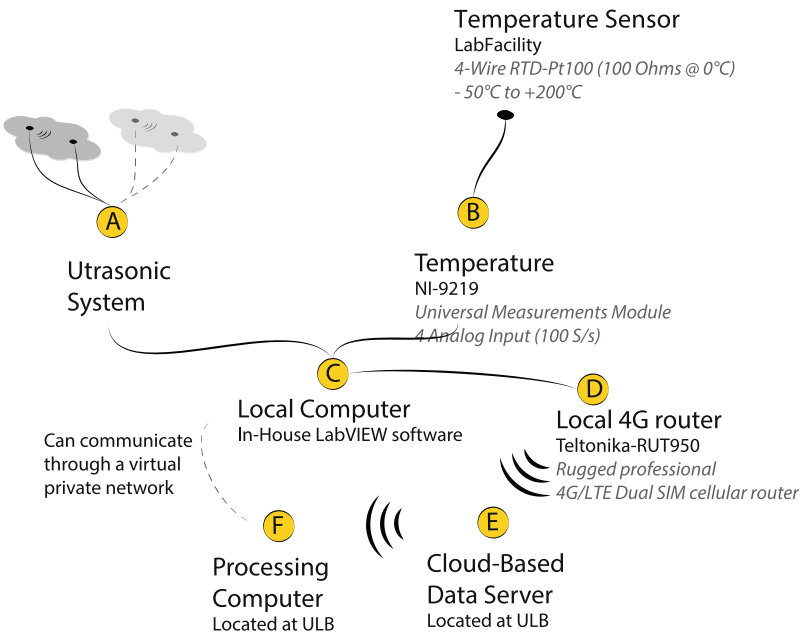

Fig. 7 General description of the instruments and connections of the full Data Acquisition and Data Transfer Chains. The Ultrasonic System is described in details in Fig. 6

3.1 Pre-processing

Each signal is first pre-processed. This mainly consists in denoising the signal using a MATLAB based soft-thresholding algorithm based on wavelet decomposition [11]. The signal is then windowed so that the crosstalk of the actuation signal is attenuated and to reduce the potential impact of the noise in the trailing part of the transient signal. The method is summarized in Fig. 9. The crosstalk between the emitted and the received signal is coming from the multiplexer board used to interrogate the different pairs of transducers successively. The use of the pre-amplifiers presented in the previous section is preventing this signal to be backpropagated to the receiver.

Fig. 8 Pictures of the monitoring system

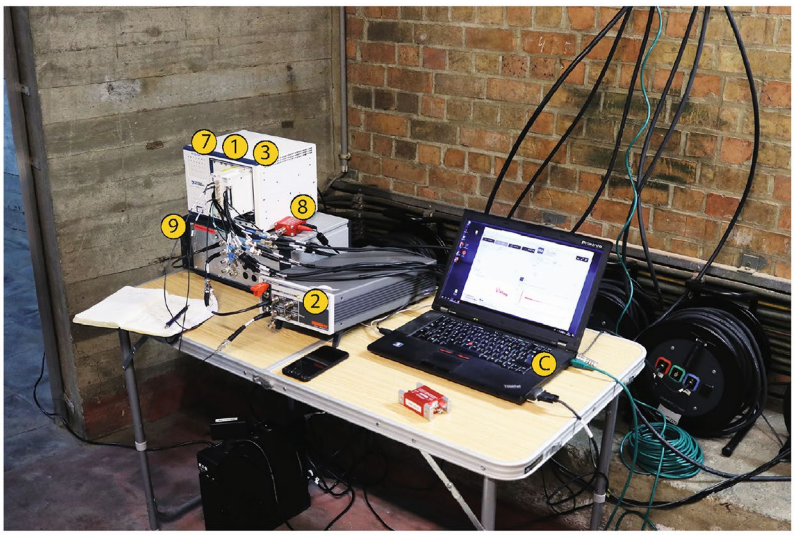

(a) Picture of the ultrasonic system and the computer located in the technical room in the immediate vicinity of the monitored zone.

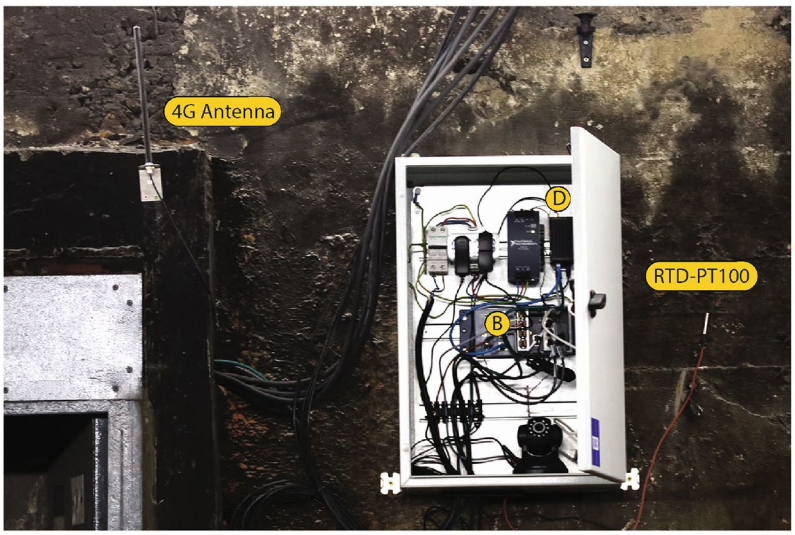

(b) Picture of the system located in the tunnel, including the 4G router.

3.2 Damage index

In a previous study [7], we developed the Direct Wave Interferometry as an alternative to the so-called Coda Wave Interferometry [12] for small specimens and lower frequencies. The distance between the emitter and the receiver where in the same order of magnitude as a transport mean free path of the ultrasonic wave propagating in the concrete specimen. This implied that the first part of the waveform could be assumed to be the ballistic wave and justified the method.

The distances between the different pairs of transducers used in the present study were much larger (from 40 to 70 cm). Such distances correspond to several transport mean free paths so that the wave has encountered several scattering events and the coherent part of the wave has most likely completely vanished when it is caught by the receiver. This implies that it cannot be assumed that the travel path of the first recorded wave corresponds to the line of sight between the emitter and the receiver and that it is not possible to track the velocity variation by simply picking the onset time. It justifies the use of a longer time window to compute the stretching factor ϵ and the related decorrelation index DCwhich are described further in the manuscript. The time window has been selected so that a large part of the energy contained in the signal is included. With such a time window, it is expected to track the relative wave velocity variation with a precision of 10^{-4} to 10^{-5}

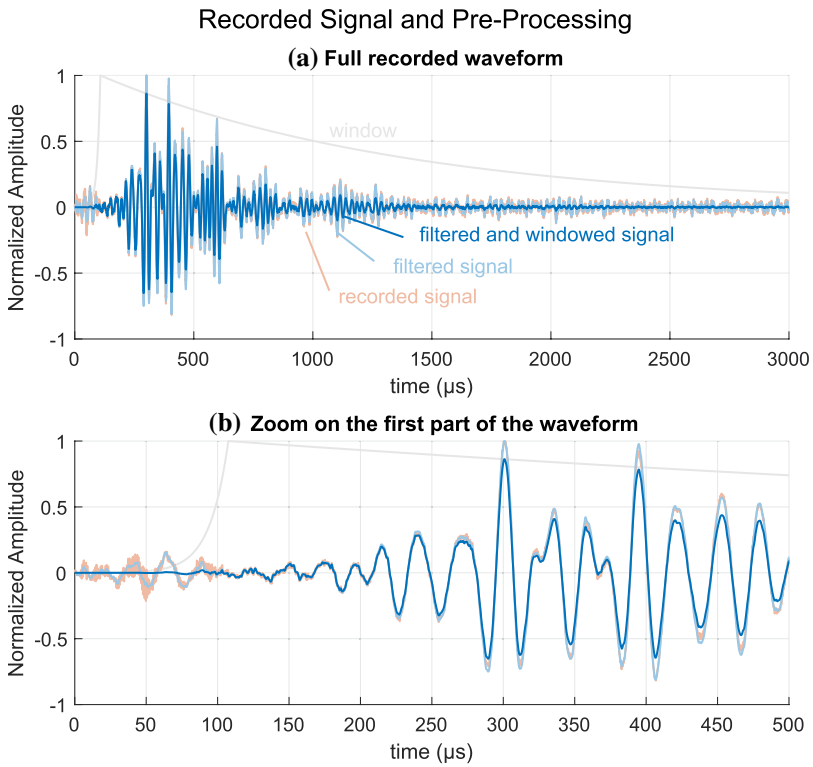

Fig. 9 Example of a recorded signal and the pre-processing applied on this signal

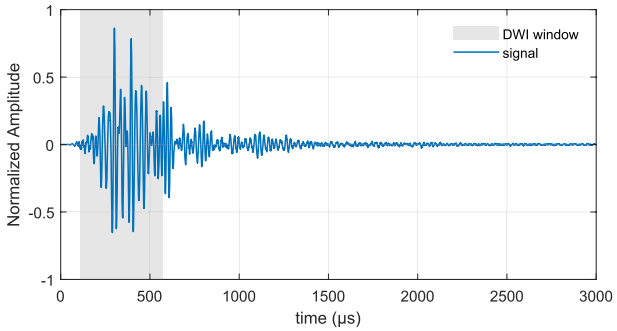

Fig. 10 Time Window on which the stretching method is applied. This time window corresponds to several mean free paths

[7]. The time window in which the stretching method is applied is presented in Fig. 10.

When the structure is subjected to environmental (e.g., temperature or humidity) or operational (e.g., stress) variations, the wave velocity is varying. For small and uniform relative wave velocity variations, the shape of the waveform is preserved and it is possible to stretch each signal $S(t)$ and find the stretching factor ϵ so that it is perfectly correlated with a reference signal, measured in reference conditions $S_0(t)$

$$\mathrm{CC}(\epsilon) = \frac{\int_{t_0}^{t_f} S(t) S_0\Big(t(1+\epsilon)\Big)\, dt}{\sqrt{\int_{t_0}^{t_f} S^2(t)\, dt \int_{t_0}^{t_f} S_0^2\Big(t(1+\epsilon)\Big)\, dt}}, \tag{1}$$

where t_0 and t_f are the initial and final time of the window in which the cross correlation is calculated. ϵ is determined by computing the minimum value of the decorrelation factor (DC = 1 − CC) using the MATLAB optimization function *fminbnd*. When the two signals are perfectly correlated DCis equal to zero and ϵ can directly be used as an estimate of the relative wave velocity variation.

A non-zero decorrelation can be related to a structural change [13], DCcan, therefore, be used as a damage indicator. Nevertheless, it only applies for smalls changes, while a larger decorrelation would lead to difficulties in estimating the relative wave velocity variation. If the two signals are not correlated anymore, the stretching factor which maximizes Eq. 1 has no physical meaning and deducing a wave velocity variation makes no sense.

In the present experiment, we have observed a large modification of the signals over time, which are due on one hand to large temperature variations and on the other hand on the hardening of the new mortar after repair. As such events strongly modify the signal waveform, it is very likely to lead to an incorrect estimate of the wave velocity variation (Fig. 11).

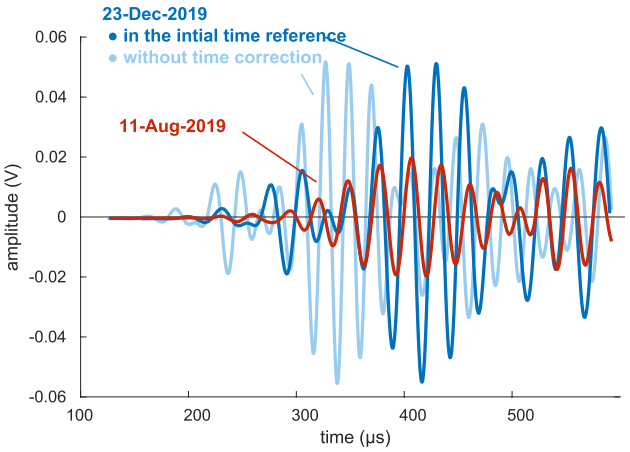

Fig. 11 Example of two signals recorded at two different periods. With time, the waveform is changing due to environmental or structural change (e.g., the ceiling repair)

To circumvent this issue, we have used a sliding reference signal. For each signal the best stretching factor is determined by minimizing the decorrelation with the average of all the signals recorded for the last 48 hours. This signal is then stacked in the queue of the last 48-h signals (FIFO style). Each signal is then kept in the same time reference which is the one of the first signal recorded (see Fig. 12). The corresponding stretching factor can, therefore, be understood as the relative wave velocity variation compared to the initial state of the structure but without having to calculate the correlation with the initial signal only. This method is expected to add robustness in the monitoring of the relative wave velocity variation since it both gets rid of the small short-term (day/night) and large long-term (seasonal or structural changes) velocity variations.

Figure 13 is presenting the evolution of the relative wave velocity variation for the first six months of the experiment on a pair of transducers (Excitation signal at 40 kHz and 80 V), using the sliding reference as described above. One can clearly see that the amplitude of the daily variations due to temperature changes is much lower that the amplitude of the variations due the structural change which is due here to the setting process of the new concrete (the skim mortar has been applied on July 24 in this region). Fig. 13 is here used as an illustrative example of the method proposed in the present paper. The results obtained on the different pairs of transducers will be presented in details in Sect. 4. The results obtained for the first two weeks of the monitoring are presented on Figure 14. The DC_{Shift}index is computed using the shifted reference as presented above (Fig. 14a) and using a fixed reference corresponding (Fig. 14b) to an overage of the signals recorded during the first two days. The figure clearly shows that using the time shifted averaged reference reduces the impact of the temperature variations (presented on (Fig. 14c) on the evolution of the DC_{Fix}index, while preserving the detection of the repair events. More specifically, using a fixed reference signal leads to higher values of the decorrelation coefficients and consequently a reduced accuracy in the estimate of the relative velocity variation. The stretching of the signal to correct for the velocity variation due to environmental factors is therefore performed based on a incorrect value. The resulting DC_{Fix} index is, therefore, much more sensitive to the temperature variations (the amplitude of the daily variations are much higher) than using a shifted reference as suggested in the present study.

In this framework, the decorrelation factor $DC_{Shift}$and the relative wave velocity variation ε have to be seen as complementary indicators. If there is no sudden changes in the

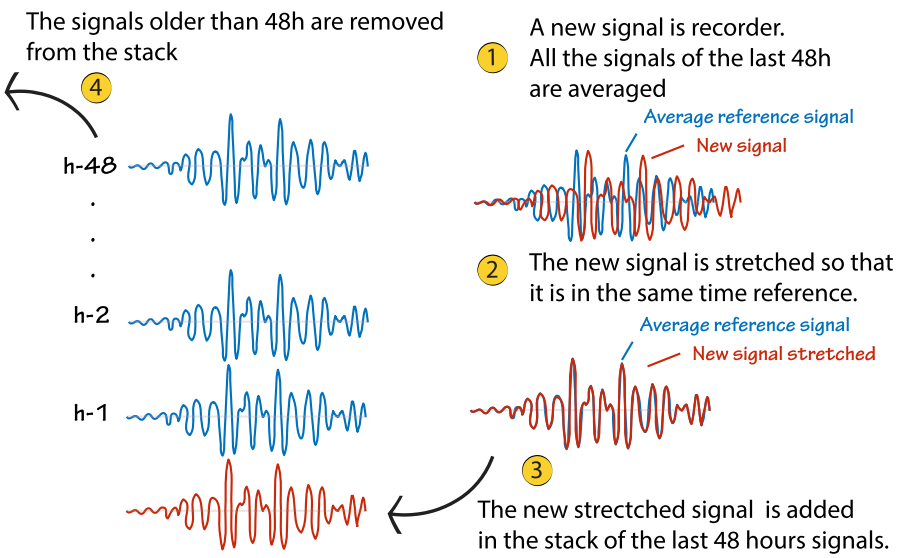

Fig. 12 Principle of the computation of the time-shifted reference

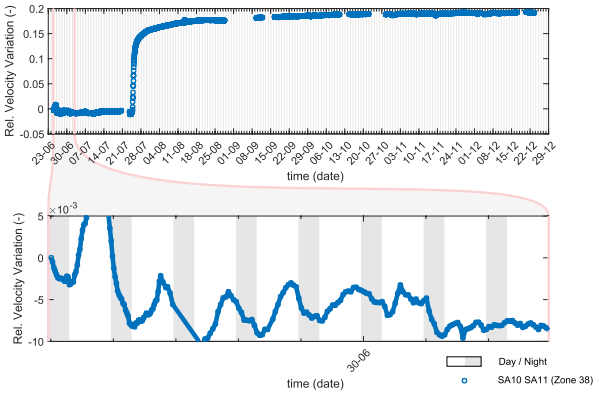

Fig. 13 Evolution of the temperature and the estimated wave velocity variations using the time-shifted reference in zone 38. The method allows to get rid of small local (day/night) and large long term (seasonal or structural changes) velocity variations. The large gaps between two successive data points correspond to periods where the system was off due to the unavailability of electrical power

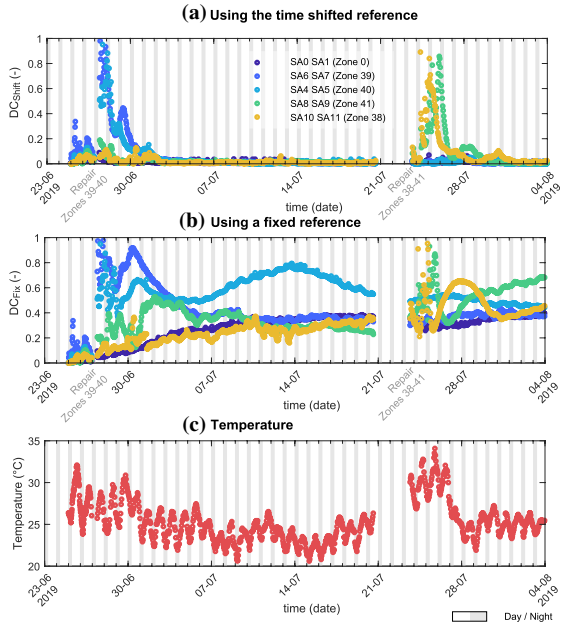

Fig. 14 Comparison between the decorrelation in a reduced period of time for the different zones (**a**) by considering the shifted reference and (**b**) a fixed reference. Shifting the reference reduces the impact of the temperature variation on the DC index

signal, the decorrelation factor remains low even if the waveform is changing. A change in DC_{Shift} is therefore indicating a fast change in the structure while a change in ϵ is indicating a long term modification. The complementarity of these indicators can help at better understanding the nature of the actual structural change. Note that when keeping a fixed reference signal rather than a shifted one, the change of DC due to environmental factors is so large that the time shifting method results in a value of ϵ which is meaningless, which also justifies the use of a shifted reference. Throughout the rest of the document, the notation DC_{Shift} will be simplified to DC.

4 Presentation of the monitoring results during an 18-month period

The results since the installation of the monitoring system in the tunnel are presented for two different periods. The first period (Sect. 4.1) is focused on the first six months after the repairs have been performed. In this period, it is expected to see the effect of the setting of the new concrete skim. Since the new concrete has been designed with a larger stiffness and better quality than the old concrete, the *P*-wave velocity in this layer is expected to be faster (and stronger). It is, therefore, assumed that after the initial setting of the skim mortar, the first arrival of the recorded wave has propagated in this layer. With this assumption, looking at wave-velocity changes in the different pairs of transducers, we are expecting to observe the typical S-shape curve which describes the setting of cement-based materials [5, 14] after repair.

After this first period, all the indicators have been re-initialized in order to focus on the study of the variation over a second period of one year. During this period, the relative velocity is expected to vary only due to environmental changes, providing there has not been any early deterioration of the repaired zones. The variation ranges in the results presented in Sect. 4.2 are therefore expected to be much more reduced in comparison to the variations observed in the first period (Sect. 4.1).

4.1 Monitoring of the setting of the concrete repair during the first 6 months after installation

As explained in Sect. 3.2, it is not possible to track directly the onset time accurately since the ballistic part of the wave seen by the sensor is expected to have completely vanished. Only the relative velocity variation is estimated using the stretching technique. The method is averaging the velocity variation along the selected time window and the actual wave path. This wave path can be different depending of the excitation signal since the scatterers to which the wave is sensitive depends on it's corresponding wavelengths. Consequently, the amplitude of the velocity variation can therefore be impacted by the type of excitation signal. The relative velocity variations presented in this sections must then be seen as a qualitative rather than a quantitative information. More specifically, the method does not allow for estimating accurately the wave velocity in the new concrete skim but can give an information on the actual hydration kinetics of the setting process and its actual degree of hydration.

Figure 15 shows the evolution of the relative wave velocity variation with time for the different excitation signals in the different zones and compared to the evolution of the temperature measured in the tunnel in the same period (from June to December 2019). The figure shows that the wave velocity variations based on the different types of waves emitted have a similar evolution with time, and are all able to identify the starting point (corresponding to the day of application of the repair in the specific zone) as well as the evolution of the hardening of the skim mortar, which tends to reach a stable value after about 28 days. Note that the amplitudes of the wave velocity changes depend strongly on the frequency signal, which is to be expected in a highly scattering material with the presence of an interface between an old concrete and a repair mortar with very different impedance characteristics. The wave velocity in the non-repaired zone has a less well-established behavior: it shows a higher variability, and an increase in the beginning of the month of August, for which we have not been able to identify the origin. It might be due to changes of stress distribution in the concrete, resulting from the repair in the other zones, but at this stages, it remains an hypothesis which is difficult to confirm. Fig 16 shows the decorrelation coefficient DCShift, which is representative of the change of the shape of the waveform during the monitoring period. The figure shows that there is a clear change after eachrepair event.

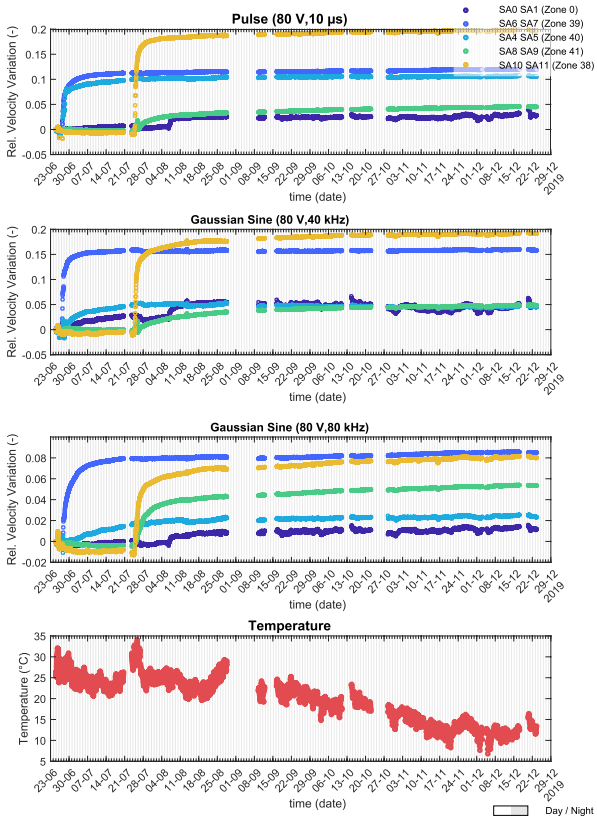

Fig. 15 Evolution of the relative wave velocity variation ε for different excitation signals compared to the temperature evolution in 2019. The amplitude of the daily variation are much lower than the variation due to the setting of the new concrete. The old concrete (Zone 0) seems more sensitive to temperature variations

4.2 Monitoring of the long-term behavior of the concrete in the repaired zones during a one-year period

Over 1 year of monitoring, the structure is subjected to large environmental variations. At the beginning of the year 2020, the winter has been mild without icing period, and two large overheating periods have been observed during the summer so that the temperature has varied over a range of almost 30°C (see Fig. 17). Unfortunately, the pair of transducers SA 1O-SA 11 (zone 38) has been lost during the month of January 2020 due to a defect in a cable. The relative velocity variations from January 2020 until December 2020 for the remaining pairs of transducers are shown in Fig. 17. The pair of transducers in the control zone 0 appears to be particularly sensitive to temperature variation. This could be related to the properties of the old concrete which might be more sensitive to temperature variations or the location in the structure. The velocity in the three other zones are also following the temperature variation. In particular, one can clearly identify the effect of the heat waves during the summer on all pairs of transducers. Figure 18 shows the DCindicators for the same period for the different transducers and excitation signals. The indicator appears to

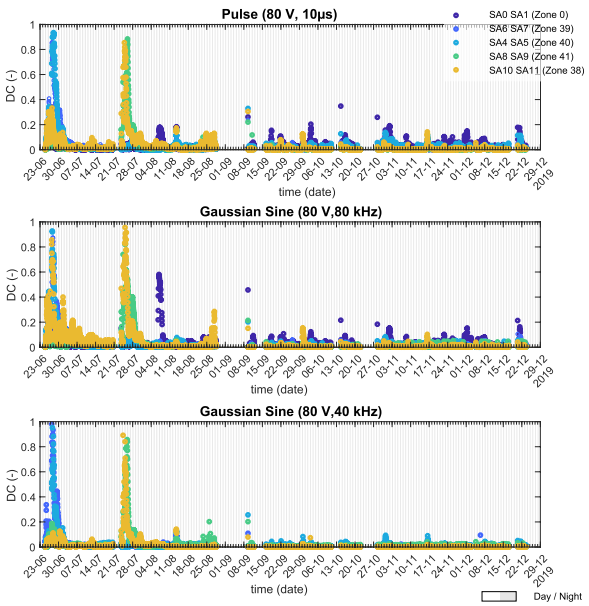

Fig. 16 Evolution of the decorrelation for different excitation signals in 2019. The DC index is mainly sensitive to the structural change induced by the repair but seems also slightly impacted by temperature variation (see Fig. 15)

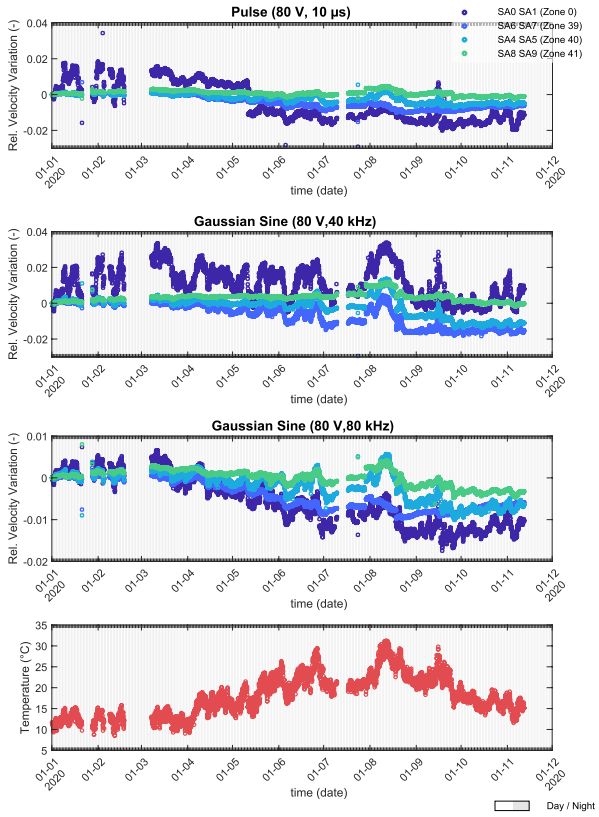

Fig. 17 Evolution of the temperature and the relative wave velocity variation ϵ for different excitation signals in 2020. The wave velocity variations appear to be correlated to the temperature variations. The old concrete (Zone 0) seems more sensitive to temperature variations

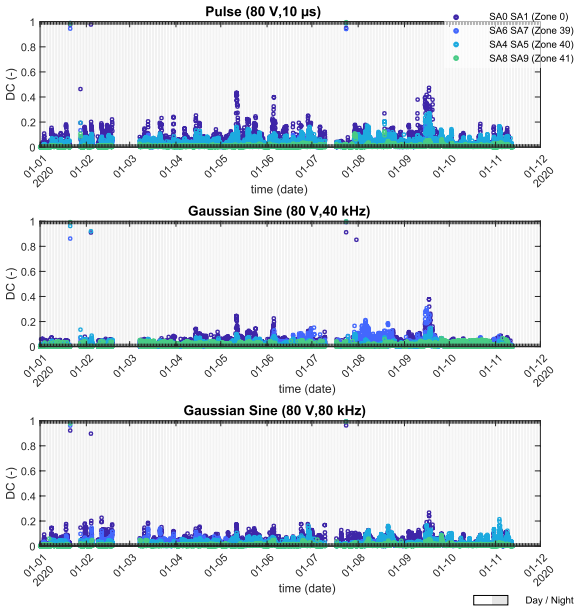

Fig. 18 Evolution of the decorrelation for different excitation signals in 2020. The index is mainly impacted by temperature variations (see Fig. 17)

be still sensitive to environmental variation; despite the use of the sliding reference and the stretching correction, which have already considerably reduced the variability. The DCindicator can reach values of up to 0.4 in the time periods corresponding to the heat waves, which is of the same order of magnitude as the values of DCobserved directly after the repair events. It can be concluded that as such, the time-shifted reference combined with time stretching is not sufficient to avoid potential false-alarms in the system under very strong changes of the environmental conditions. The following section is, therefore, dedicated to the development of statistical processing strategies to filter out the remaining environmental effects from the results, and obtain a more robust monitoring strategy.

5 Improvement of the monitoring system through advanced statistical analysis

Figure 14 shows that the stretching method allows for increasing significantly the robustness of DCto environmental variations, but that for some time periods, it is not sufficient to compensate for all the variations (Fig. 18). This could cause false alarms in the system, which is highly undesirable in practical applications. One way to improve the robustness of the system is to take advantage of the potential statistical correlation between the different indicators computed, which are all subjected at the same time to the same environmental changes, while the potential failure events are likely to be isolated and, therefore, uncorrelated as seen from the different pairs of transducers.

An efficient tool to remove the observed trends in multivector data is the use of the Mahalanobis squared distance, as detailed in [15] and shortly recalled below.

5.1 The Mahalanobis squared distance

We consider the multivariate feature vector made of the DC values computed on all the pairs (except in zone 38 where the signal was lost for a long period due to a damaged cable), and for the different excitation signals, from January 2020 to December 2020. This results in a vector of 12 features (4 zones and 3 types of excitation signals), recorded every two hours during that period.

The Mahalanobis squared distance is a statistical measure that reduces the multivariate feature vector to a single scalar value by comparing it to the mean value of the samples. This scalar value can then be used to perform novelty detection as in [15]. The computation of the Mahalanobis squared distance is based on the estimation of the mean and the covariance matrix $[C]_{n\times n}$ of the multivariate features vectors which is made of n(=12 here)-features

vectors $\{y_i\}$ of which N samples $y_{\xi i}$ are measured. The covariance matrix is given by:

$$C_{ij} = \frac{1}{N-1}\sum_{\xi=1}^{N}\left(y_{\xi i}-\bar{y}_i\right)\left(y_{\xi j}-\bar{y}_j\right), \tag{2}$$

where $\bar{y}_i$ is given by

$$\bar{y}_i = \frac{1}{N}\sum_{\xi=1}^{N} y_{\xi i}. \tag{3}$$

If the features are independent, the matrix is diagonal. It is generally not the case if the different features are affected by the same factors, and this is an interesting property to filter out environmental data.

A spectral decomposition of the covariance matrix can be performed to project the features on a basis where $[C]_\eta$ is diagonal. This is achieved with a singular value decomposition of the matrix $[C]$ [15]

$$[U][S][V]^T = [C], \tag{4}$$

where $[U]$ and $[V]$ are, respectively, the matrices of the left and right singular vectors which verify the orthogonality conditions $[U]^T[U] = [V]^T[V] = [I]$. Note that because matrix $[C]$ is square and symmetric, $[U] = [V]$.

$[S]$ is the singular values matrix of which the diagonal terms are the variance σ_i^2 in the principal axis. The features $\{y_i\}$ are then projected into the subspace of the left singular vectors

$$\{\eta_i\} = \{U_i\}^T[y], \tag{5}$$

so that, as demonstrated in [15], the Mahalanobis squared distance D_ξ^2 of the sample ξ can be expressed as

$$D_\xi^2 = \sum_{i=1}^{n}\frac{1}{\sigma_i^2}\left(\eta_{\xi i}-\bar{\eta}_i\right)^2, \tag{6}$$

where $\bar{\eta}_i$ is the mean the vector $\{\eta_i\}$

$$\bar{\eta}_i = \frac{1}{N}\sum_{\xi=1}^{N}\eta_{\xi i}. \tag{7}$$

Equation 6 shows that the contribution of the left singular vectors to the Mahalanobis squared distance is inversely proportional to the square of their respective singular values: the more a singular vector contributes to the variability in the data (high associated singular value), the less it contributes to the Mahalanobis squared distance. If the data used to compute the covariance matrix contain variability mostly due to the environment, then this contribution is naturally filtered out by the Mahalanobis squared distance.

Figure 19 shows the standard deviations σ_i corresponding to the different singular values of the covariance matrix computed on a random set of 40 % of all samples of measurements during the year 2020. It can be observed that the first value is much larger than the others, indicating that the effect of the corresponding factor can be filtered out naturally with the Mahalanobis squared distance. To illustrate this, the value of D_ξ^2 is computed with a covariance matrix estimated on a random subset of 40% of the full set of multivariate feature vectors over the one year period and represented in Fig. 21. The evolution of D_ξ^2 is much less sensitive to environmental variations than the individual features which show large variations corresponding to very high temperatures in the tunnel, showing the possibility to filter out environmental variability and make the monitoring system more robust.

5.2 Alarm threshold

The second stage in the statistical analysis consists in defining an alarm threshold regarding a given indicator. In the present study, the proposed univariate indicator is the Mahalanobis squared distance as shown in Fig. 21.

Warning levels are traditionally defined by assuming a certain type of distribution of the monitored multivariate or univariate features and defining the parameter which controls the percentage of false-positives (confidence level). In practice, the probability density functions of such features are hardly perfectly known so that the method often fails to establish an accurate threshold. Another difficulty is also that the confidence levels used in structural health monitoring are usually very high and the established threshold is, therefore, very dependent on the tails of the distributions, which are often not well described by the assumed probability density function of the features, as there are only a limited number of sample points in these tails.

As an alternative, extreme value statistics (EVS) [16] can be used to define more robust thresholds. It relies on the

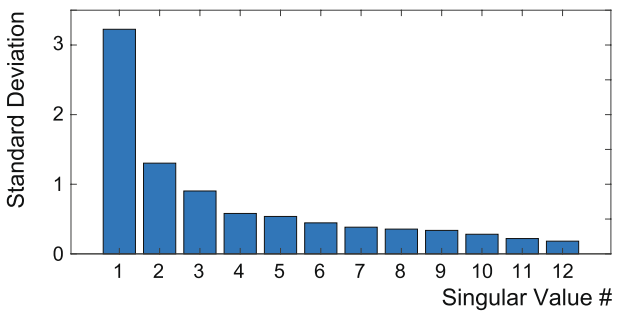

Fig. 19 Spectral decomposition of the covariance matrix. The first singular value is predominant which indicates that the corresponding statistical correlation will be filtered out in the Mahalanobis squared distance

the extreme value theorem (EVT). The first step consists in fitting a parametric model to the right tail of the empirical cumulative density function (CDF) of the training data. When looking at the distribution of maxima, there are only three possible distributions: the Gumbel, Weibull and Frechet distributions [17]. The three of them must be tested to find the actual distribution which fits best the data. The method has been tested to define a robust threshold to detect the exact time of crack initiation during a loading test on a concrete beam monitored using embedded ultrasonic transducers in [18].

The distribution which is most suitable in our application was found to be the the Frechet which is expressed by

$$H(x) = \begin{cases} \exp\left(-\frac{\delta}{x-\lambda}\right)^{\beta} & \geq 0 \\ 0 & \text{otherwise,} \end{cases} \tag{8}$$

where λ and δ and β are parameters to be estimated from the tail of the distribution. The threshold level T_{EVS} for a confidence level α is obtained by inverting Eq. 8 to find

$$T_{EVS} = x \ : \ H(x) = 1 - \alpha/2. \tag{9}$$

The procedure which has been chosen to fit the actual distribution was differential evolution (DE), an evolution-based optimization algorithms [19]. A normalized mean square error between the the fitted distribution and the empirical cumulative distribution function (CDF) is used as a cost function. The process is explained in more details in [18, 20, 21], and the code is implemented in Matlab and has been shared and developed by our colleagues from the Dynamics Group in the University of Sheffield.

To define a robust threshold, a subset of the training data used initially to compute the covariance matrix (which consists in a random subset of 40% of all the data) is used. It contains the 40% of this data set corresponding to the highest values of the Mahalanobis squared distance (blue dots in Fig. 21). It can be seen that the tail of the determined Frechet cumulative distribution function nicely fits the empirical cumulative distribution function (Fig. 20). Two threshold alarms have been defined. They, respectively, correspond to degrees of confidence of 99% and 99.9%. 1% and 0.1% of outliers are therefore accepted without triggering an alarm (see Eq. 9). To validate that the thresholds are well defined, Mahalanobis squared distance is computed on all samples to verify that the ratio of outliers remains in the defined degree of confidence. Figure 21 shows that the ratio of false positives computed on all the data is, respectively, 0.9% for the 99% threshold and 0.012% for the 99.9% threshold which are very closed to the tuning parameters. This is indicating that the thresholds values are well defined, thanks to the EVS method and that no extreme events have been observed in the recorded data.

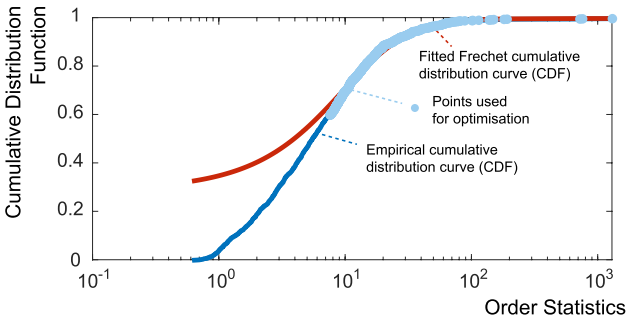

Fig. 20 Extreme Value Statistics processing: Frechet Distribution curve-fit on the 40% largest training data using the a Differential Evolution algorithm fitting. The training data correspond to 40% randomly distributed data among all the data

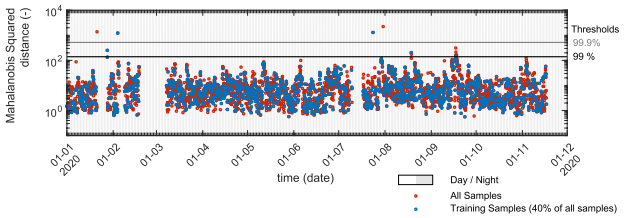

Fig. 21 Mahalanobis squared distance computed on the DCindexes. The thresholds at 99% and 99.9% are obtained using a Frechet distribution fitted on the tail of the cumulative distribution function of the Malahanobis squared distance (Fig. 20). The ratio of false-positives are, respectively, 0.9% for the 99% threshold and 0.12% for the 99.9% threshold.

It is now suggested to determine the thresholds as exposed above but on a reduced period of time Fig. 22. The major difference with the results shown in Fig. 21 is that both the covariance matrix and the thresholds T_{EVS} are estimated based on the data of the first 5 months of 2020, instead of the whole year. The large variations of temperature observed in the summer are, therefore, not included. It can be observed that the ratio of false positives on the full set of data is increasing to 5.48% for the 99% threshold and 2.18% for the 99.9% threshold. Such values are clearly over the thresholds and the alarm is triggered. This highlights the importance of computing the Mahalanobis squared distance to filter out the environmental effects on a sufficiently representative period to design a robust alarm threshold.

5.3 Filtering of the individual features

The Mahalanobis squared distances gives a global indication of the evolution of the twelve features monitored over the one-year period in the tunnel. By setting appropriate alarm levels as illustrated above, it is possible to establish if a significant structural change has occurred in one of the monitored areas, but not to locate in which area the structural

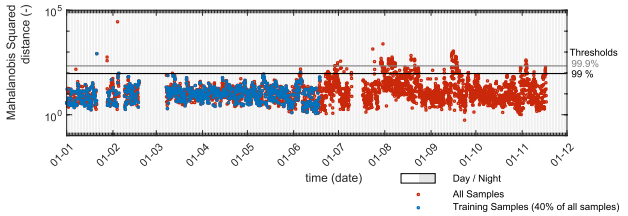

Fig. 22 Mahalanobis squared distance computed on the DCindexes. The threshold at 99% and 99.9% are obtained using a Frechet distribution fitted on the tail of the cumulative distribution function of the Malahanobis squared distance of the first 5 months of 2020 (blue circles). The ratio of false positives are, respectively, 5.48% for the 99% threshold and 2.18% for the 99.9% threshold, which are higher than the prescribed confidence levels

change occurred. The approach for performing such a localization consists in reprojecting the measured features from the transformed space using the left singular vectors of the covariance matrix, after removal of the identified variability linked to the highest singular values. This is done by reverting the projection in the principal axis Eq. 5 as follows

$$\{y_i\} = \{U_i\}[\eta]. \tag{10}$$

If all the terms are kept in the principal vectors, Eq. 10 is simply giving the unfiltered features. To filter out the environmental effect in each feature vector $\{y_i\}$, it is suggested to weight the contribution of each feature in the singular value axis $\{\eta_i\}$ according to its relative contribution in the total variance

$$\{\eta_i'\} = \{\eta_i\} \frac{1/\sigma_i^2}{\sum_{i=1}^{n} 1/\sigma_i^2}, \tag{11}$$

where $\{\eta_i'\}$ is the i^{th} weighted feature in the singular values axis so that filtered features in the original axis $\{y_i'\}$ can be expressed as

$$\{y_i'\} = \{U_i\}[\eta']. \tag{12}$$

This weighting is similar to the one applied to compute the Mahalanobis squared distance (Eq. 6). The method has been applied on the DCindexes from January 2020 until December 2020, using again a random subset of 40% of the data over the whole year to compute the covariance matrix. The resulting individual features are shown in Fig. 23 where it can be observed that compared to the unfiltered values of DCpresented in Fig. 18, the indexes are barely impacted by environmental effects, demonstrating the high efficiency of the approach. Where the Mahalabonis squared distance allows to have a global monitoring of all the features, re-projecting the values of DCin the original axis after weighting allows to filter out very efficiently the remaining variability in the data. A representative example of alarm thresholds

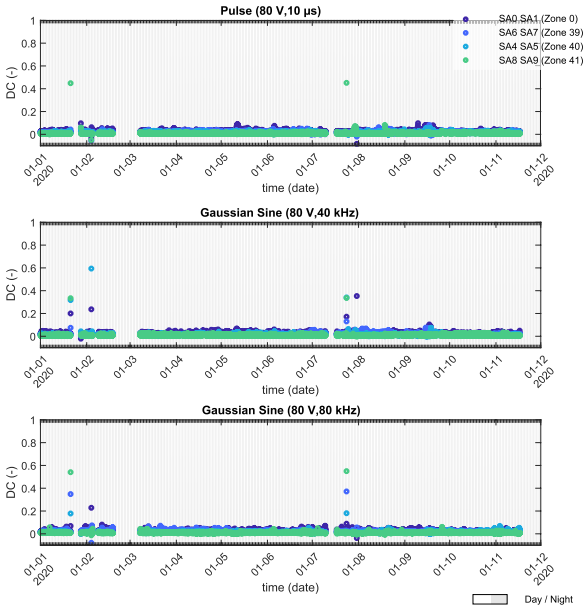

Fig. 23 Evolution of the filtered decorrelation for different excitation signals in 2020. Compared to the unfiltered indexes presented in Fig. 18, the indexes are barely impacted by the environmental effects

computed on the tail of the distribution (EVS) of a DCindex is shown on Fig. 24, using the same approach and same percentage of data to fit the Frechet distribution as above. The ratios of false positives for both thresholds remain in the degrees of confidence, and no false alarm is given by the system.

6 Conclusion and outlooks

A permanent monitoring system has been installed in the Rogier tunnel in Brussels in June 2019. It consists of 5 pairs of embedded ultrasonic piezoelectric transducers of which four pairs are situated in an area where repair to the concrete ceiling has been performed during the monitoring period.

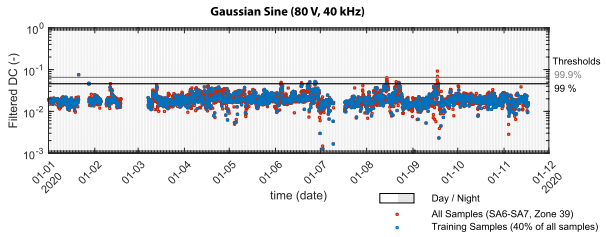

Fig. 24 Example of EVS applied on a filtered DCindex. The threshold alarm at 99% and 99.9% are obtained using a Frechet distribution fitted on the tail of the cumulative distribution. The ratio of false positives is, respectively, 0.75% for the 99% threshold and 0.09% for the 99.9% threshold

The system is fully automated and is sending recorded signals regularly to a cloud server in our laboratory. From the recorded ultrasonic signals, several indicators are computed to follow the state of health of the repaired concrete zones.

The monitoring has been performed over an 18-month period, and is still running at the time of writing this article. During the first 6 months, repairs have been done in four of the monitored areas. Our results demonstrate that the indicators we are computing are able to detect precisely the moment when the repair mortar was applied, and to follow its hardening over a 28-day period. The monitoring of these indicators over the period of the first six months shows that the quality of the repair was steady over time and that there was no problem of cavities forming at the interface between the old concrete and the skim mortar. A first contribution of this paper is the modification of the feature extraction from the raw signals involving a reference signal shifted in time, rather than a fixed reference signal. We have shown how this new approach is efficient to decrease the very high variability observed in our indicators due to environmental changes when using a fixed reference as in previous work, despite the use of a time stretching technique.

A second monitoring period of one year, from January 2020 to December 2020 has then been studied. Despite the use of the shifted reference, it was shown that our indicators still suffer from the influences of the environment, in particular in time periods where the temperature was very high in the tunnel. We have, therefore, proposed a statistical method to further filter out the environmental effects. The technique is based on observed correlations between the features extracted in the different zones in the tunnel, and has been shown to be very effective to filter out the remaining environmental variability. In addition to this filtering technique, we have also presented a method based on extreme value statistics to set the thresholds for alarm triggering. A first threshold is set on a global indicator of damage based on the Mahalanobis squared distance computed on all the individual features measured. This can give an indication that an abnormal event has occurred.

To determine in which area this event has occurred, we have proposed a technique which consists in reexpanding the data in the initial feature space after identification and filtering of the environmental effects based on training data. It was shown that after this process, the individual features corresponding to each zone were very robust to environmental changes, and that it was possible to set an individual threshold on each of them in order to determine the location were a structural change has occurred.

During this study, potential alternative methods to filter out the environmental variability have been identified and are worth studying in the future. These include the use of dynamic time warping [22] as an improvement of the simple time stretching method, and the use of non-linear ultrasonics [23, 24] to enhance the relative sensitivity of the indicators to damage and environmental changes. Non-linear ultrasonic testing is, however, difficult with the current monitoring system due to the length of the cables used, so that a modification of the hardware should be studied. Another possibility is to use non-linear techniques to filter out the environmental effects [25, 26], rather than a linear one as the one based on the Mahalanobis squared distance.

Finally, monitoring of the features over time will continue in the tunnel and will allow us to check if the monitoring period used in the current study is sufficient to cover all the possible environmental changes that the tunnel will see in the long term, or if an update of the filtering techniques is necessary at some point.

Acknowledgements The authors would particularly like to thank Vincent Thibert from the Brussels regional agency for mobility (Brussels Mobility) for his confidence in the project and for letting us the access to the tunnel. The authors have also greatly appreciated the kind support of Prof. Keith Worden on the statistical aspects of this work, including sharing the associated software.

Data Availability Statement The data of the monitoring system used in the present paper may be shared upon email request with researchers interested in developing novel ideas and methods.

Declarations

Conflict of interest The authors declare that they have no conflict of interest.

References

1. Blanchard J (2013) Masterplan pour la mise en sécurité et la rénovation des tunnels routiers gérés par la Région de Bruxelles-Capitale. Regional Public Service Brussels Mobility, Regional Public Service Brussels Mobility, Tech. rep
2. Dumoulin C, Deraemaeker A (2017) Design optimization of embedded ultrasonic transducers for concrete structures assessment. Ultrasonics 79:18. https://doi.org/10.1016/j.ultras.2017.04.002
3. Deraemaeker A, Dumoulin C (2020) Piezoelectric Ultrasonic Transducer Embedded in Concrete Structures, Pending Patent 20183481.9-1001
4. Song G, Gu H, Mo YL (2008) Smart aggregates: multi-functional sensors for concrete structures-a tutorial and a review. Smart Materials and Structures 17(3). https://doi.org/10.1088/0964-1726/17/3/033001
5. Dumoulin C, Karaiskos G, Carette J, Staquet S, Deraemaeker A (2012) Monitoring of the ultrasonic P-wave velocity in early-age concrete with embedded piezoelectric transducers. Smart Materials and Structures 21(4). https://doi.org/10.1088/0964-1726/21/4/047001
6. Dumoulin C, Karaiskos G, Sener JY, Deraemaeker A (2014) Online monitoring of cracking in concrete structures using embedded piezoelectric transducers. Smart Materials and Structures 23(11). https://doi.org/10.1088/0964-1726/23/11/115016
7. Deraemaeker A, Dumoulin C (2019) Embedding ultrasonic transducers in concrete: a lifelong monitoring technology. Construction

Build Materials 194:42. https://doi.org/10.1016/J.CONBUILDMAT.2018.11.013
8. Tsangouri E, Karaiskos G, Aggelis D, Deraemaeker A, Hemelrijck DV (2015) Crack sealing and damage recovery monitoring of a concrete healing system using embedded piezoelectric transducers, Structural Health Monitoring **14**(5). https://doi.org/10.1177/1475921715596219
9. Grosse C, Ohtsu M (2008) Acoustic Emission Testing (Springer. Berlin Heidelberg, Berlin, Heidelberg. https://doi.org/10.1007/978-3-540-69972-9
10. Ziehl P, ElBatanouny M (2015) Low-level acoustic emission (AE) in the long-term monitoring of concrete, In: *Acoustic Emission (AE) and Related Non-destructive Evaluation (NDE) Techniques in the Fracture Mechanics of Concrete: Fundamentals and Applications*, pp. 217–236. https://doi.org/10.1016/B978-1-78242-327-0.00011-8
11. Donoho D (1995) De-noising by soft-thresholding. IEEE Trans Inform Theory 41(3):613. https://doi.org/10.1109/18.382009
12. Planès T, Larose E (2013) A review of ultrasonic Coda Wave Interferometry in concrete. Cement Concrete Res 53:248. https://doi.org/10.1016/j.cemconres.2013.07.009
13. Planès T, Larose E, Margerin L, Rossetto V, Sens-Schönfelder C (2014) Decorrelation and phase-shift of coda waves induced by local changes: multiple scattering approach and numerical validation. Waves in Random and Complex Media 24(2):99. https://doi.org/10.1080/17455030.2014.880821
14. Delsaute B, Boulay C, Granja J, Carette J, Azenha M, Dumoulin C, Karaiskos G, Deraemaeker A, Staquet S (2016) Testing Concrete E-modulus at Very Early Ages Through Several Techniques: An Inter-laboratory Comparison. Strain 52(2):91. https://doi.org/10.1111/str.12172
15. Deraemaeker A, Worden K (2018) A comparison of linear approaches to filter out environmental effects in structural health monitoring. Mechanical systems and signal processing 105:1. https://doi.org/10.1016/j.ymssp.2017.11.045
16. Castillo E (1988) Extreme value theory in engineering (Academic Press. San Diego. https://doi.org/10.1016/c2009-0-22169-6
17. Fisher RA, Tippett LH (1928) Limiting forms of the frequency distribution of the largest or smallest member of a sample. Math Proc Cambridge Philosoph Soc 24(2):180. https://doi.org/10.1017/S0305004100015681
18. Deraemaeker A, Dumoulin C, Dervilis N, Cross EJ, Worden K (2019) Statistical analysis of damage indicators based on ultrasonic testing with embedded piezoelectric transducers, SMART 2019 - IX ECCOMAS Thematic Conference on Smart Structures and Materials pp. 251–262
19. Storn R, Price K (1997) Differential evolution—a simple and efficient Heuristic for Global Optimization over continuous spaces. J Global Opt 11(4):341. https://doi.org/10.1023/A:1008202821328
20. Worden K, Manson G, Sohn H, Farrar C (2005) Extreme value statistics from differential evolution for damage detection, Conference Proceedings of the Society for Experimental Mechanics Series
21. Worden K, Allen D, Sohn H, Stinemates D, Farrar CR (2002) Extreme Value Statistics for Damage Detection in Mechanical Structures. Tech. rep, Los Alamos National Laboratory
22. Douglass AC, Harley JB (2018) Dynamic time warping temperature compensation for guided wave structural health monitoring. IEEE Trans Ultrasonics Ferroelectrics Frequency Control 65(5):851. https://doi.org/10.1109/TUFFC.2018.2813278
23. Zhang Y, Tournat V, Abraham O, Durand O, Letourneur S, Le A, Lascoup B (2017) Nonlinear coda wave interferometry for the global evaluation of damage levels in complex solids. Ultrasonics 73:245. https://doi.org/10.1016/j.ultras.2016.09.015
24. Shokouhi P, Rivière J, Lake CR, Le Bas PY (2017) Dynamic acousto-elastic testing of concrete with a coda-wave probe: comparison with standard linear and nonlinear ultrasonic techniques, T. Ulrich, Ultrasonics 81(2017):59. https://doi.org/10.1016/j.ultras.2017.05.010
25. Sohn H, Worden K, Farrar C (2001) Novelty detection using auto-associative neural network, in Proc 2001 ASME Int. Mech Eng, Congress and Exposition, New York, USA
26. Lämsä V, Kullaa J (2007) Dynamical extension of nonlinear factor analysis in structural health monitoring to remove environmental effects, in Proceedings of III ECCOMAS Thematic Conference on Smart Structures and Materials. Gdansk, Poland